

The Influence of Welding Parameters on the Nugget Formation of Resistance Spot Welding of Inconel 625 Sheets



HAMID REZA REZAEI ASHTIANI and ROOZBEH ZARANDOOZ

A 2D axisymmetric electro-thermo-mechanical finite element (FE) model is developed to investigate the effect of current intensity, welding time, and electrode tip diameter on temperature distributions and nugget size in resistance spot welding (RSW) process of Inconel 625 superalloy sheets using ABAQUS commercial software package. The coupled electro-thermal analysis and uncoupled thermal-mechanical analysis are used for modeling process. In order to improve accuracy of simulation, material properties including physical, thermal, and mechanical properties have been considered to be temperature dependent. The thickness and diameter of computed weld nuggets are compared with experimental results and good agreement is observed. So, FE model developed in this paper provides prediction of quality and shape of the weld nuggets and temperature distributions with variation of each process parameter, suitably. Utilizing this FE model assists in adjusting RSW parameters, so that expensive experimental process can be avoided. The results show that increasing welding time and current intensity lead to an increase in the nugget size and electrode indentation, whereas increasing electrode tip diameter decreases nugget size and electrode indentation.

DOI: 10.1007/s11661-015-3030-1

© The Minerals, Metals & Materials Society and ASM International 2015

I. INTRODUCTION

RESISTANCE spot welding (RSW) is one of the most important methods for sheet metal welding being used in many industries such as the automobile, aerospace, electronics, *etc.* Compared with other welding processes such as arc welding processes, RSW is fast, easily maintained, and automated. This welding process includes coupled interactions of electrical, thermal, metallurgical, and mechanical phenomena and even surface behaviors. Because of this complexity, it is difficult to obtain insightful information on the welding process through experiments alone. In recent years, numerical method provides a powerful and reliable technique for studying these interactions and prediction in the welding processing industry, and, at the same time, costly experimental process can be avoided.

Strength and quality of the welds of RSW are defined by size and shape of weld nuggets. In general, there is a direct correlation between heat generation and nugget size in RSW process. The contact resistances at the faying surface between workpieces, welding time, current density, and sheet thickness principally determine the heat generation during welding and the subsequent nugget shape and size.^[1]

Nickel-based superalloy Inconel 625 was developed as a solid solution-strengthened alloy containing relatively

high levels of chromium, molybdenum, carbon, and niobium. It is widely employed in aerospace, marine, chemical, and petrochemical applications, due to its excellent mechanical properties, fatigue strength, oxidation resistance, weldability, and resistance to high-temperature corrosion on prolonged exposure to aggressive environments.^[2,3] To obtain a superior performance, a better understanding of spot welding processes of Inconel 625 has become necessary and the control of weld quality is much more essential. Also, in experimental methods, it is not possible to obtain a perfect model of temperature distribution, stresses, and deformation in whole welding zone, so the numerical modeling has proven to be an effective method in understanding the RSW process, and more research is needed to better understanding the thermal and mechanical behaviors of materials.

Spot welding was recognized in the late nineteenth century and it was used for joining plates since 1920.^[4] Nied^[5] introduced an FE model for RSW process in ANSYS commercial software, then investigated the effect of the electrode geometry on the workpiece deformation and stresses as a function of temperature, and verified its results with experimental results of welding AISI 316 materials. A three-dimensional transient heat transfer model has been developed to predict temperature distribution during RSW by Wei and Ho.^[6] In a similar research, Tsai *et al.*^[7] simulated the generated heat of RSW process and investigated the effects of different thickness and dissimilar materials on temperature distribution and nugget shape. The iterative method to simulate spot welding with flat-tipped electrodes has been employed by Vogler and Sheppard.^[8] Darwish *et al.*^[9]

HAMID REZA REZAEI ASHTIANI, Assistant Professor and ROOZBEH ZARANDOOZ, Student of Master Degree, are with the School of Mechanical Engineering, Arak University of Technology, Arak, Iran. Contact e-mails: hr_rezaei@just.ac.ir; hr_rezaei@arakut.ac.ir

Manuscript submitted August 5, 2014.

Article published online July 1, 2015

have suggested a statistical model for RSW of aluminum plates that investigated the effects of current, time, electrode force, and plate thickness on the welding strength. A thermomechanical model to analyze sheet deformation during RSW process of aluminum alloys was represented by Sun and Dong.^[10] Kim *et al.*^[11] determined the distributions and changes of the contact pressure at both the faying surface and the electrode-workpiece interface with a thermo-elastic-plastic finite element analysis. They measured the stress and strain distributions in the weldment and their changes during the RSW process. The electrical potential, temperature, and residual stress distributions during different stages and welding parameters such as heat input and welding time of RSW with an electro-thermo-mechanical FE model have been studied by Serajzadeh *et al.*^[12] Eisazadeh *et al.*^[1] have presented an incremental finite element model for parametric study of nugget size in RSW process. They have investigated the effects of contact resistance and electrode force on nugget size and shape. Lei *et al.*^[13] created a two-dimensional finite element model for RSW process of mild steel with three sheets assemblies and discussed under appropriate welding contact condition and other experimental physical parameters. Moshidi and Sattari-Far^[14] developed a 2D axisymmetric electro-thermo-mechanical finite element model to study the effect of welding time and current intensity on nugget size in RSW process of AISI type 304L austenitic stainless steel sheets using ANSYS commercial software package. Although there are various investigations on the modeling of RSW process,^[15–18] more studies are still useful to reach a better understanding of electro-thermo-mechanical behavior of materials during and after the process. To the best of the authors' knowledge, there is no research dealing with welding of Inconel 625 sheet by RSW reported in the literature.

In the present study, the phenomenon of nugget formation and the effect of RSW process parameters on size and shape of weld nuggets, temperature distribution, and weldability of Inconel 625 sheet are studied.

The effects of welding time and current intensity on the temperature of faying surface and electrode indentation are investigated. The predicted weld nugget sizes are compared with the metallographic test results to verify the accuracy of the model. These results can be used to optimize the RSW parameters of Inconel 625 sheets.

II. EXPERIMENTAL PROCEDURE

A. Material

Inconel 625 sheets of 0.7 mm thickness were selected as the base metal for this investigation. The chemical composition of the investigated superalloy has been given in Table I. Samples with equal dimensions of

145 mm × 40 mm for investigating weldability lobe and 40 mm × 40 mm for simulation verification were provided and cleaned before welding, using sandpapers Nos. 400 and 600. Class II copper-chromium-zirconium electrode from RWMA group A was used in this study, and an electrode re-dressing was performed periodically.

B. Specimen and Welding Parameters

Specimens were welded using a pneumatic phase-shift controlled pedestal-type RSW machine. The power supply was a calibrated 50 Hz sine wave AC current with a capacity of 100 kVA. To investigate the effects of welding current and time on the nugget size and the weldability lobe diagram, according to ANSI/AWS/SAE/D8.9-97,^[19] six series of test specimens of the same material were welded. As shown in Table II, welding times are chosen fixed and welding currents are varied in any series. After welding, the weldability lobe diagram was revealed by some peel tests to determine the upper and lower limits of welding current and time for RSW, as shown in Figure 1 (for CA2).

The weldability lobe diagram obtained for this investigation is shown in Figure 2. Since expulsion is a complicated phenomenon and is not considered in the FE model, the best parameters for experiments are those which give the widest range without any expulsion. As it is clear in Figure 2, welding current values from 6 to 7 kA provide the widest range of acceptable welding time, and welding time of 10 cycles, in addition to providing a wide range of acceptable current, provides a weld nugget in a low welding current. Therefore, for verifying simulation results, welding time of 10 cycles is selected as a fixed parameter and other selected parameters are represented in Table III.

Table II. Welding Parameters Used for Investigating the Weldability Lobe Diagram

| Electrode Tip Diameter = 4.7 mm, Electrode Force = 3.3 kN, Holding Time = 5 cycle | | |
|---|----------------------|----------------------|
| Test No. | Welding Time (Cycle) | Welding Current (kA) |
| CA1 | 6 | 4-9 |
| CA2 | 8 | 4-9 |
| CA3 | 10 | 4-9 |
| CA4 | 12 | 4-9 |
| CA5 | 16 | 4-9 |
| CA6 | 20 | 4-9 |

Table I. Chemical Composition of the Employed Inconel 625

| C | Nb | Mo | Fe | Cr | Ni | Ti | Al | Co | Cu | Si | Mn | Mg |
|-------|------|------|-----|-------|-------|-----|------|-------|------|------|-------|-------|
| 0.032 | 2.87 | 8.61 | 4.4 | 21.67 | 59.28 | 0.2 | 0.18 | 0.124 | 0.05 | 0.07 | 0.024 | 0.035 |

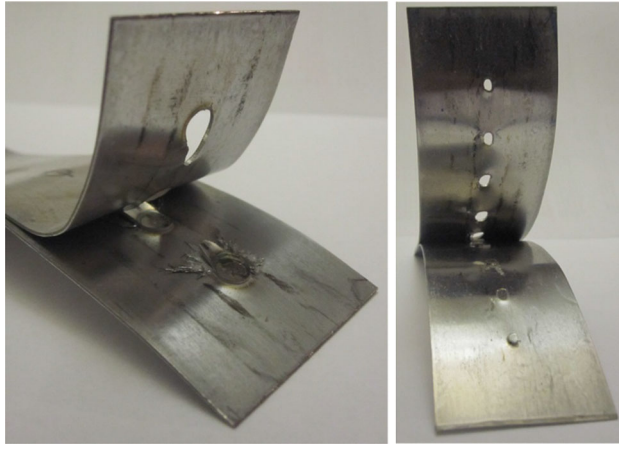


Fig. 1—Sample of peel test for the specified weldability lobe diagram.

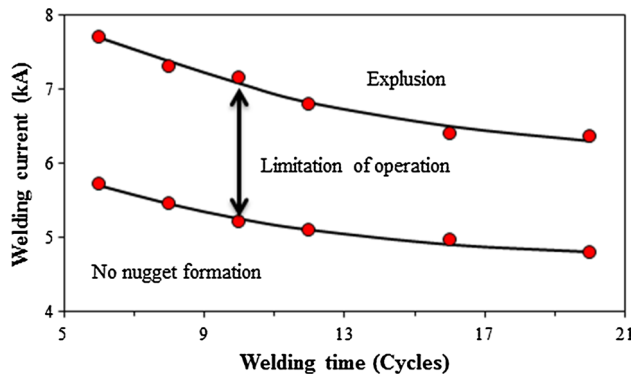


Fig. 2—Weldability lobe diagram of Inconel 625 for 3.3 kN electrode force determined by peel testing.

Table III. Welding Parameters Used for Simulation Verification

| Welding Parameters | Value |
|-----------------------------|--------------------|
| Electrode tip diameter (mm) | 4.7 |
| Electrode force (kN) | 3.3 |
| Welding current (kA) | 6–7 |
| Squeeze time (cycle) | 50 (cycle = 20 ms) |
| Welding time (cycle) | 10 (cycle = 20 ms) |
| Holding time (cycle) | 5 (cycle = 20 ms) |
| Sheet thickness (mm) | 0.7 |

C. Weld Nugget and Penetration Measurement

The joint quality between two welded sheets is often described by the nugget shape and size of weld. Nugget size and indentation depth can be measured by the metallographic test. Three samples from each trial were measured to get the weld nugget size and indentation depth. After RSW, samples (consisting of weld centerline) were prepared for metallographic examination using standard metallography procedures. In this study, 100 ml HCl, 100 ml H₂O, and 40 ml H₂O₂ (30 pct), which is the recommended etchant for Nickel alloy

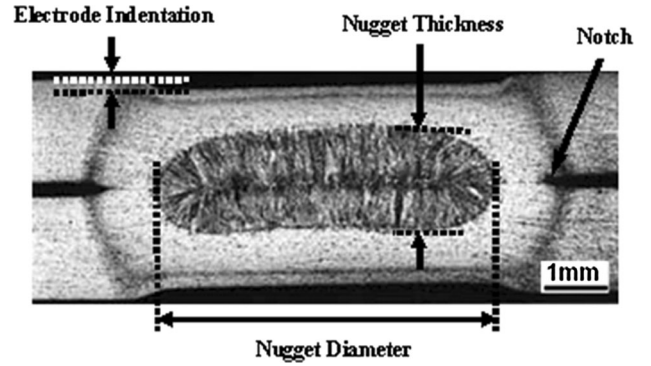


Fig. 3—The weld nugget areas and the indentation depth.

according to ASTM E 340-00 (Reapproved 2006),^[20] have been used for macrography and investigation of the nugget size. Figure 3 illustrates the measured areas of the welded joints.

III. DEVELOPMENT OF MATHEMATICAL MODEL

A. Governing Equation

The governing equation for calculation of the heat generation in a certain period is given by Eq. [1]:^[12]

$$Q = RI^2t, \quad [1]$$

where I , R , and t are the electrical current, electrical resistivity, and time, respectively. The governing equation for axisymmetric transient thermal analysis and calculation of the heat generation per unit volume is given by^[21]

$$\rho C \frac{\partial T}{\partial t} = \frac{\partial}{\partial r} \left(k \frac{\partial T}{\partial r} \right) + \frac{k}{r} \frac{\partial T}{\partial r} + \frac{\partial}{\partial z} \left(k \frac{\partial T}{\partial z} \right) + \dot{q}_v, \quad [2]$$

where r and z are, respectively, radial and axial coordinates; ρ , C , T , t , and K are density, specific heat, temperature, time, and thermal conductivity, respectively; and \dot{q}_v is the rate of internal heat generation. The governing equation of the electrical analysis is^[21]

$$\frac{\partial}{\partial r} \left(C_e \frac{\partial \varphi}{\partial r} \right) + \frac{C_e}{r} \frac{\partial \varphi}{\partial r} + \frac{\partial}{\partial z} \left(C_e \frac{\partial \varphi}{\partial z} \right) = 0, \quad [3]$$

where C_e is the electrical conductivity and φ is the electrical potential. The coupled thermal-electrical problem is solved by the following matrix equation:^[21]

$$\begin{bmatrix} [C'] & [0] \\ [0] & [0] \end{bmatrix} \begin{Bmatrix} \{ \dot{T} \} \\ \{ \dot{V} \} \end{Bmatrix} + \begin{bmatrix} [K'] & [0] \\ [0] & [K''] \end{bmatrix} \begin{Bmatrix} \{ T \} \\ \{ V \} \end{Bmatrix} = \begin{Bmatrix} \{ Q \} \\ \{ I \} \end{Bmatrix}, \quad [4]$$

where $[K']$ the thermal conductivity matrix; $[C']$ is the thermal specific heat matrix; $[K'']$ is the electric coefficient matrix; $\{Q\}$, $\{V\}$, $\{I\}$, and $\{T\}$ are the vectors of heat flow, electric potential, current vector, and temperature, respectively.

For the structural analysis, the stress equilibrium equation is given by^[21]

$$\nabla\sigma(r, t) + b(r, t) = 0, \quad [5]$$

where b , σ , and r are body force, stress, and coordinate vectors, respectively.

The constitutive equation of the materials based on the thermo-elastic-plastic theory is given by^[14]

$$d\{\sigma\} = [D^{ep}]d\{\varepsilon\} - \{C\}dT \quad [6]$$

$$\{C\} = -[D^e] \left(\{\alpha\} + \frac{\partial[D^e]^{-1}}{\partial T} \{\alpha\} \right), \quad [7]$$

where $\{\sigma\}$, $\{\alpha\}$, and $\{\varepsilon\}$ are vectors of stress, thermal expansion coefficient, and strain, respectively, and $[D^e]$ and $[D^{ep}]$ are matrixes of elastic stiffness and elastic-plastic stiffness, respectively, where $[D^{ep}] = [D^e] + [D^p]$.^[13]

B. Boundary Conditions

As shown in Figure 4, two types of boundary conditions are defined in the FE model of RSW analysis under the electro-thermal boundary conditions and the mechanical boundary conditions.

1. Thermo-electrical boundary conditions

In this study, it is assumed that the electrical current is applied uniformly to the top of the electrode and the

bottom of the lower electrode and is set to be zero for the reference electrical potential. Also it is assumed that the far end of the sheets is at ambient temperature 298 K (25 °C) and water temperature inside the copper electrode is 298 K (25 °C). However, it should be mentioned that in RSW process thermal radiation and convection with air have small effect on cooling compared with conduction. This is due to small heating zone and short period of the spot welding process. But for more accuracy, as for the heat transfer to the surrounding air during the electro-thermal analysis, convection and radiation are both taken into consideration and their combined effect is represented in the following two equations for the temperature-dependent heat transfer coefficient, h :^[22]

$$h_{\text{total}} = \begin{cases} 0.0668T \left(\frac{W}{m^2}\right) & 0^\circ\text{C} < T < 500^\circ\text{C} \\ 0.231T - 82.1 \left(\frac{W}{m^2}\right) & T > 500^\circ\text{C} \end{cases} \quad [8]$$

$$q = h_{\text{total}}(T_s - T_{\text{sur}}). \quad [9]$$

The most important property in the simulation of RSW process is the contact resistivity of faying surface. During the RSW process, the contact resistance is a function of hardness, temperature, electrode force, and surface condition, and increases with decreasing electrode force and increasing hardness and number of contact spots at interfaces. Hardness decreases with increasing temperature. Interactions between these factors affecting the change of electrical resistance during spot welding are accounted.^[23] Therefore, this is a

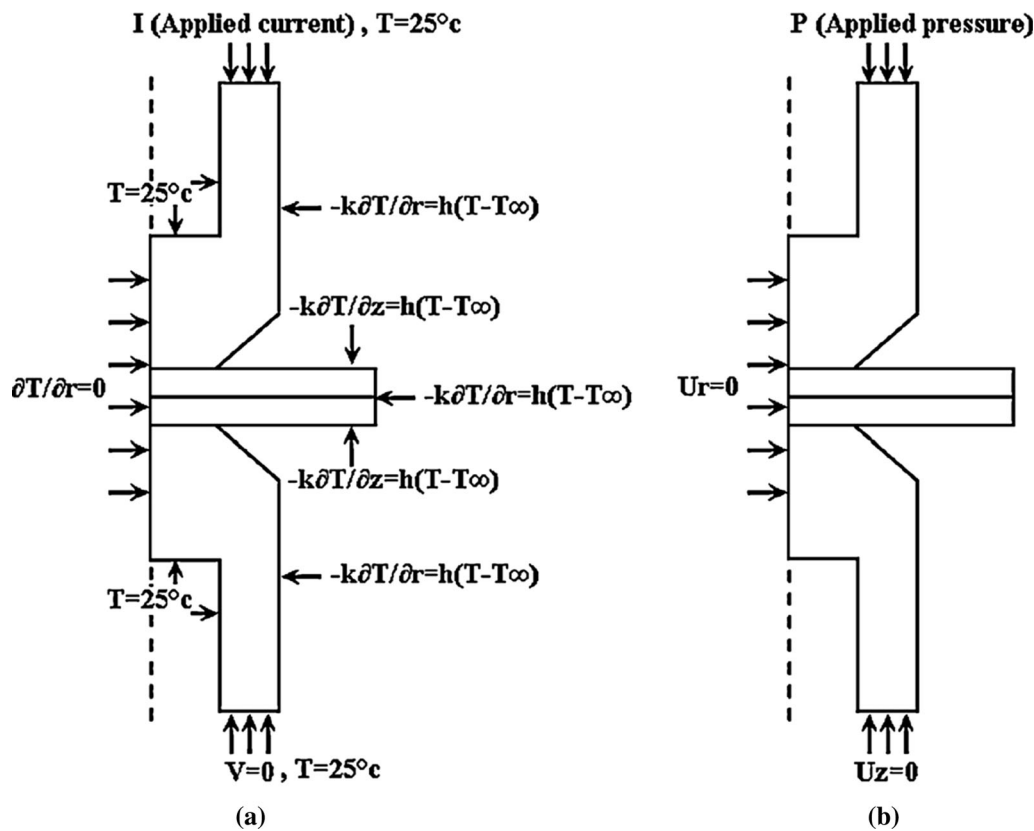


Fig. 4—Schematic of the (a) electro-thermal boundary conditions and (b) mechanical boundary conditions.

highly non-linear problem involving the complex interaction between thermal, electrical, and mechanical phenomena. To simplify the problem, many researchers take the contact resistivity as a function of temperature. This simplification is reasonable because, firstly, the load is constant in a specified RSW process; secondly, the yield strength of the materials, which determines the contact status in the contact area, is essentially influenced by temperature. With this simplification, the computing time can be greatly reduced. Therefore, in this study, the temperature-dependent contact resistance is imposed on the faying surface, and due to the small amount of workpiece/electrode contact resistance compared with workpiece/workpiece contact resistance, this factor was ignored and the contact resistance between the workpieces is determined using the formulation developed by Sun *et al.*^[10]

$$\sigma_g = \frac{1}{\rho h} = \frac{1}{R_C A_C} = \frac{I}{2\sqrt{L(T_s^2 - T_0^2)}\pi r_c^2}. \quad [10]$$

Here, L is the Lorentz constant (L is found to be around $2.4 \times 10^{-8} \text{ (V/K)}^2$ for most metals), T_s is the solidus temperature of the interface, and T_0 is the interface absolute temperature. The contact radius r_c for the electrode–sheet interfaces and the faying interface is extracted from the previous mechanical analysis results.

2. Mechanical boundary condition

Uniformly distributed pressure for the given electrode force is applied to the top of the upper electrode. Contact pairs are set up between the electrode-to-sheet interface and the sheet-to-sheet faying interface, respectively. This ensures that the surfaces in contact will not penetrate each other. The temperature history obtained from the electrical–thermal analysis is imposed as thermal loading, and the symmetry line of the model allows extending only along the vertical axis, with no lateral displacement.

IV. NUMERICAL TECHNIQUE

A. Model Geometry and Meshing

In this work, a computational model based upon the finite element ABAQUS program is developed to describe the electrical–thermal–mechanical mechanism of the RSW process. In applying the FEM to the modeling of RSW, the joint geometry (*i.e.*, sheet and electrode) is represented by a two-dimensional axisymmetric model. As shown in Figure 5, quadratic quadrilateral axisymmetric elements (*i.e.*, CAX8R for mechanical and DCAX8E for electro-thermal) are used to model the electrode and Inconel sheets. In order to correctly couple and transfer data, the model must have identical mesh both in the electrical–thermal analysis and in the elastic–plastic analysis, whereas the element types are different or have different degree of freedom options. As shown, the grid is graded from fine to coarse, according to the expected reduction in temperature gradient on moving away from the heat source. In

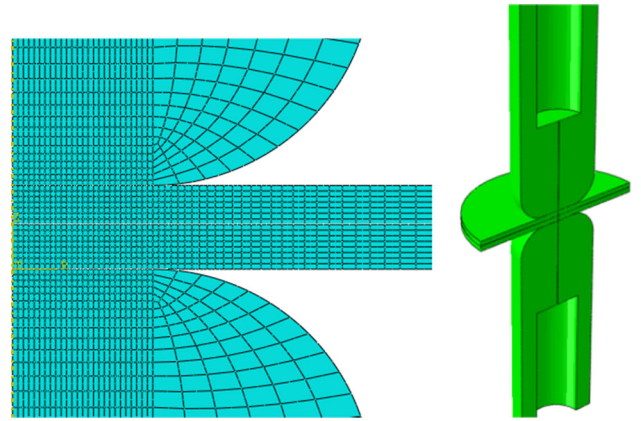


Fig. 5—Geometric model for resistance spot welding.

order to predict accurate results, temperature-dependent physical, mechanical, and electrical properties of the materials are to be used for both electro-thermal and mechanical analyses.

B. Computational Procedure

The RSW process starts with analyzing the squeeze cycle in which the electrode force is applied to the electrodes by a mechanical analysis. The results of this mechanical analysis include initial deformations, contact radius and area, and root opening, which passed on to the electro-thermal analysis. In this stage, the temperature distribution by the Joule heating is calculated from the fully coupled electrical–thermal finite element analysis. In the electrically thermally coupled analysis after the electrical and thermal boundary conditions applied to the model, the solving routine performs the calculations of joule heating at the workpiece–workpiece and electrode–workpiece faying surfaces, as well as in the electrode and base material. Solid-to-liquid and liquid-to-solid phase changes are included in the model using the definition of melting and solidus temperature and latent heat. As a result, the temperature distributions are obtained in the electrical–thermal analysis and sent to the mechanical analysis as a nodal thermal load. The deformed area of the electrode and sheet assembly and contact pressure are the results of mechanical analysis that obtain a new contact condition. So, the mechanical results are given to electro-thermal analysis to update contact conditions for the following incremental analysis. This loop continues until the welding time is complete. Figure 6 shows the computation procedure for modeling the coupled electro-thermal analysis and uncoupled mechanical analysis of the RSW process in the flowchart.

V. RESULTS AND DISCUSSION

The physical weld attributes such as weld nugget size and weld penetration are the most important parameters governing the mechanical performance and weld quality of RSW. Welding current, welding time, and electrode

tip diameter significantly affect these characteristics. For instance, volume of melted metal is a function of heat input which is controlled by the welding parameters including welding current and welding time.^[24] Based on this concept, the FE model was employed to simulate the RSW process in order to quantitatively understand the effects of the process parameters on the temperature distribution and the nugget size at different conditions. In this study, nugget formation in RSW process is predicted and compared with experimental data. A comparison between measured shapes of weld nugget from experiment and the calculated results from FEM simulation at a welding current of 7 kA and a welding time of 10 cycles is shown in Figure 7. The comparison of simulation and experimental results for nugget

diameter at different welding currents is shown in Figure 8. As it is clear, there is a good agreement between the two sets of results except at higher current

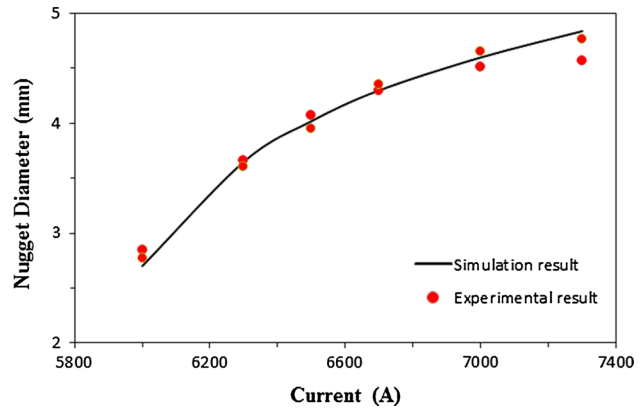


Fig. 8—Comparison of simulation and experimental results for nugget diameter at different welding currents.

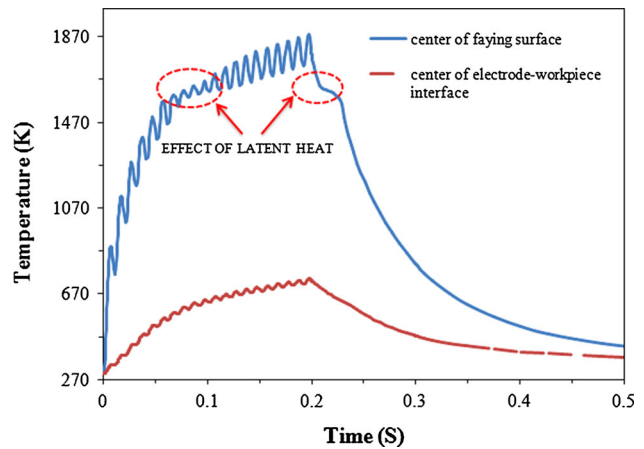


Fig. 9—Temperature histories at two locations in RSW process (10 cycles and 6.5 kA).

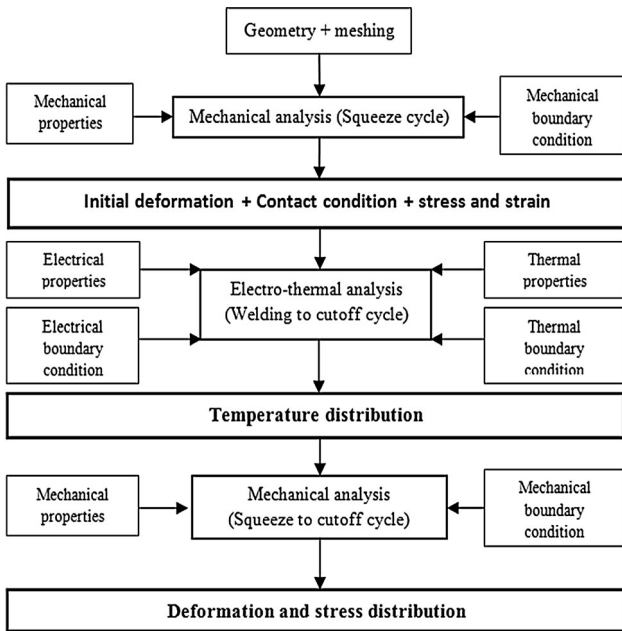


Fig. 6—The finite element solving algorithm used for simulating the RSW process.

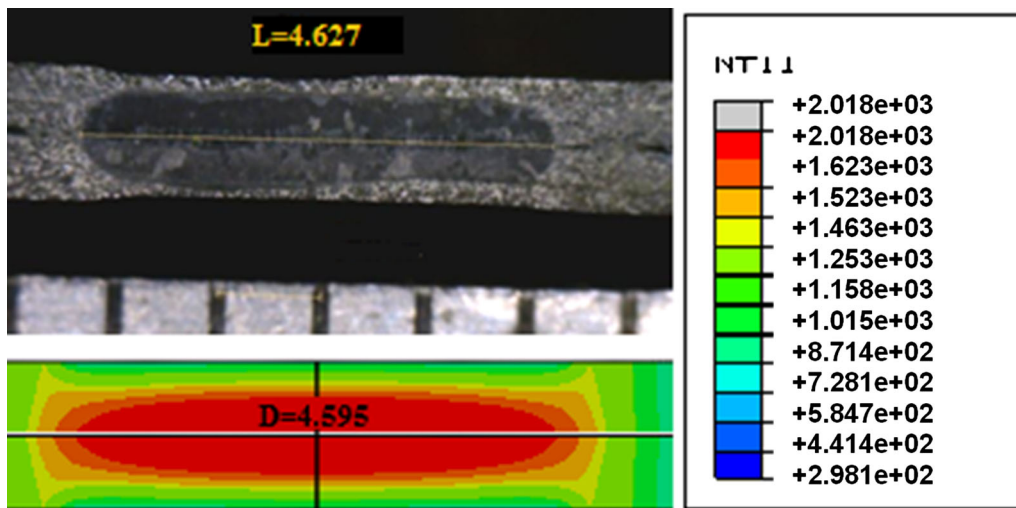


Fig. 7—Comparison of (a) simulation and (b) experimental results at the 10 cycles and 7 kA.

that expulsion occurs in the experimental results. Figure 9 shows the temperature history during the RSW process of specimen, at two locations: the center of the nugget and the center of electrode and workpiece interface. It is clear that the highest temperature is always at the center of faying surface during the whole RSW process. In addition, the temperature of the faying surface is higher than that of the electrode-sheet interface; similarly these results have been reported by Eisazadeh *et al.*^[1] This condition has demonstrated the effect of latent heat at the melting temperature [1623 K (1350 °C)] and also points out that considering latent heat in FE model causes temperature raise slowly at melting point. The region which endures the melting temperature during welding process is determined as weld nugget. Melting will first occur at the faying surface and then expand to the lateral and the vertical directions in the next 2 to 3 cycles.

The temperature distribution along the faying surface at the end of welding cycles is shown in Figure 10, which illustrates the geometry of the nugget and the heat-affected zone (HAZ). This diagram is employed to measure the nugget width where the horizontal axis represents the distance from the center of the nugget. Weld quality is often stated in terms of weld nugget diameter.

Investigations of results and the Joule heating formula (Eq. [1]) show that the welding current has the

greatest effect on the generation of heat at faying surface. Therefore, it is a primary control variable in RSW process. Figures 11 and 12 show the effect of welding current on nugget diameter and thickness in RSW process, respectively. At the start of the diagrams, the weld nugget size increases very fast, but the rate of increase of weld nugget size is reduced when the welding current becomes larger and the nugget size raises until

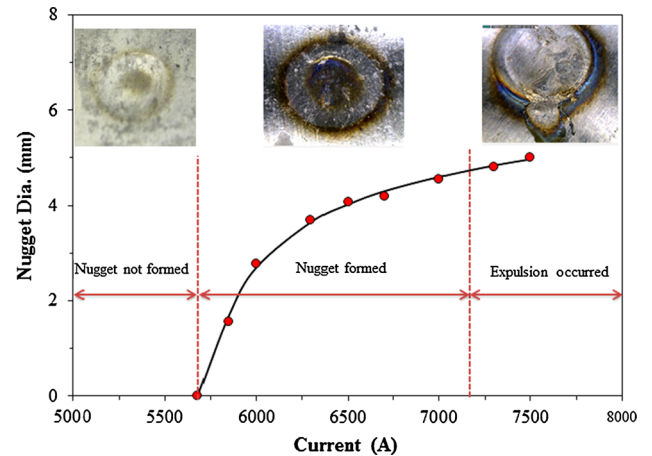


Fig. 11—Effect of welding current on nugget diameter; welding time is 10 cycles and electrode tip diameter is 4.7 mm.

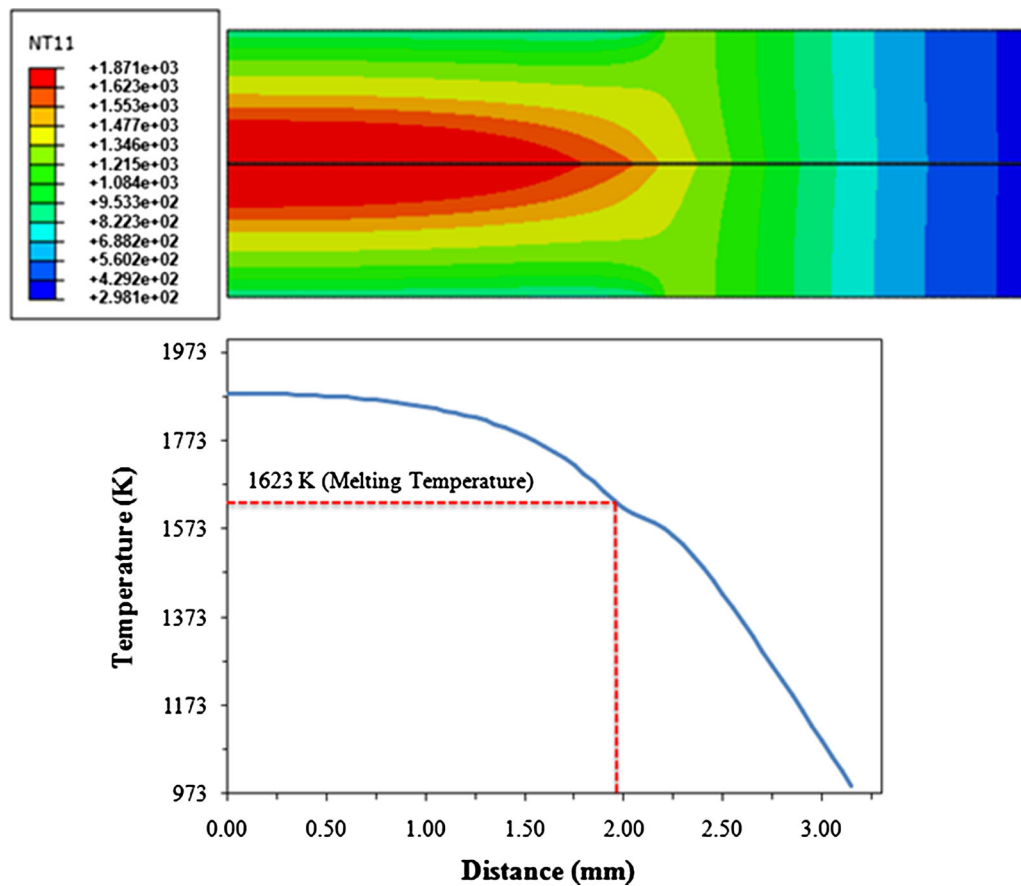


Fig. 10—Temperature distributions along the faying surface employed to measure the nugget diameter (10 cycles and 6.5 kA).

melt spattering occurs, as these conditions have been reported in RSW of AISI type 304L austenitic stainless steel sheets by Moshayedi and Sattari Far.^[14] This happens due to the fact that the area of contact between

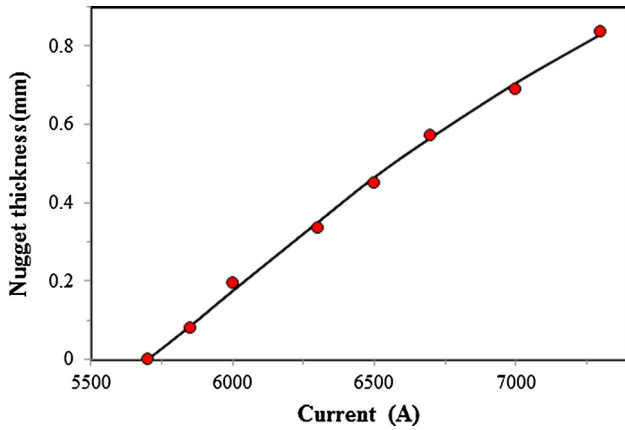


Fig. 12—Effect of welding current on nugget thickness; welding time is 10 cycles and electrode tip diameter is 4.7 mm.

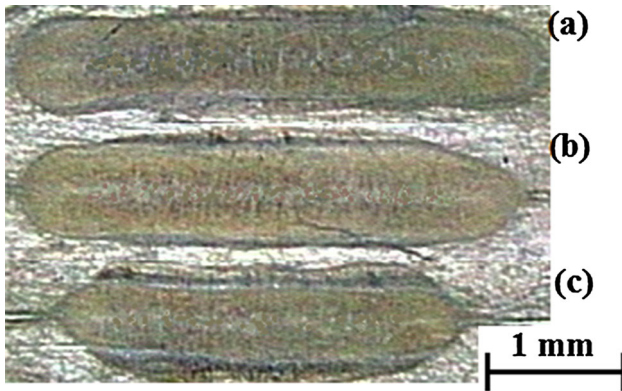


Fig. 13—Variations of nugget dimension for different welding currents of (a) 7.15, (b) 6.1, and (c) 5.4 kA, at a welding time of 10 cycles and an electrode tip diameter of 4.7 mm (experimental results).

the sheets increases when the weld nugget size increases, and at the same time both the electrical and thermal conductivities will decrease with the rising temperature. According to Eq. [10], with increasing temperature due to increasing welding time or welding current, contact resistance, which is the dominant parameter in controlling heat generation, decreases because of increasing of T_0 . In other words, the contact area at faying surface of the sheets becomes larger, and therefore the current intensity reduces with increasing the weld nugget size. This causes the decrease of contact resistance. Moreover, the liquid metal during nugget formation is squeezed to turn into a spatter under the action of the excessive resistance heat generated by the large welding heat and electrode force, and this phenomenon is called expulsion. When expulsion occurs, diameter and thickness of nugget are reduced abruptly due to melt spattering from weld pool. The effects of expulsion on nugget growth are not taken into account in the FEM, but increasing welding current can cause heavier expulsion, as the result of experimental test. Comparison between Figures 11 and 12 also indicates that the effect of welding current on nugget thickness is more than its effect on nugget diameter.

As it is clear from the experimental results (Figure 13), welding current has significant effect on the nugget dimensions in RSW process.

Figures 14 and 15 show the interaction effect of welding current and welding time on nugget diameter and thickness, respectively. As it is clear from these figures, with increasing the welding time, the rate of increase of weld nugget size is reduced, due to the fact that a longer welding time causes more heat losses from the weld zone by conduction and convection; so it reduces the effect of welding time on nugget growth due to heat generation.^[14] This phenomenon does not considerably occur with increasing welding current (since the welding time is constant), and thus it can be seen that the nugget growth rate reduction with increasing welding current is less than that with increasing welding time (Figures 14 and 15). These diagrams

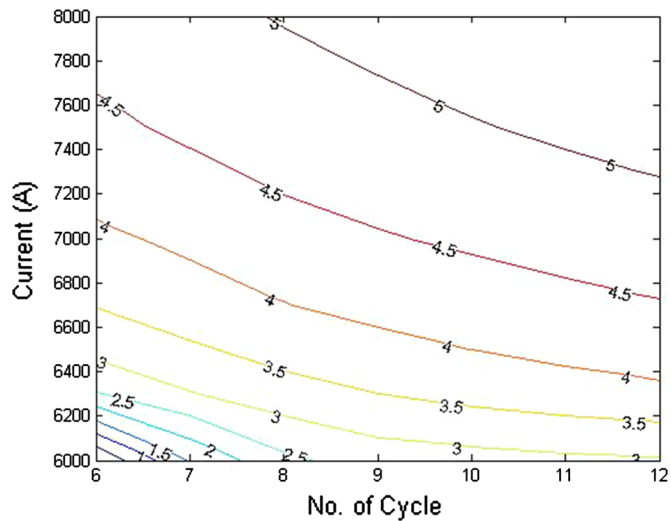
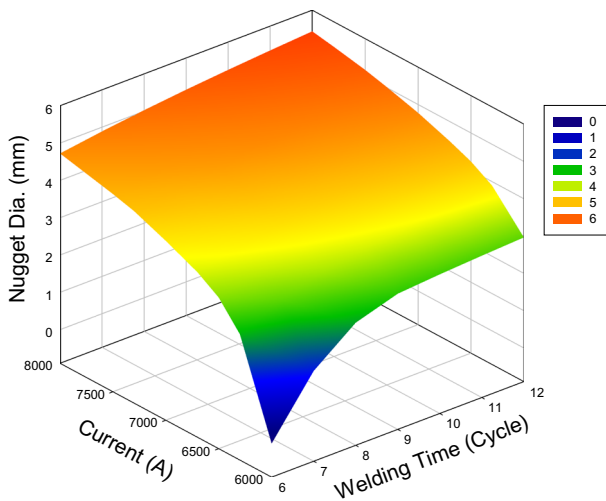


Fig. 14—Interaction between welding time, welding current, and nugget diameter with an electrode tip diameter of 4.7 mm.

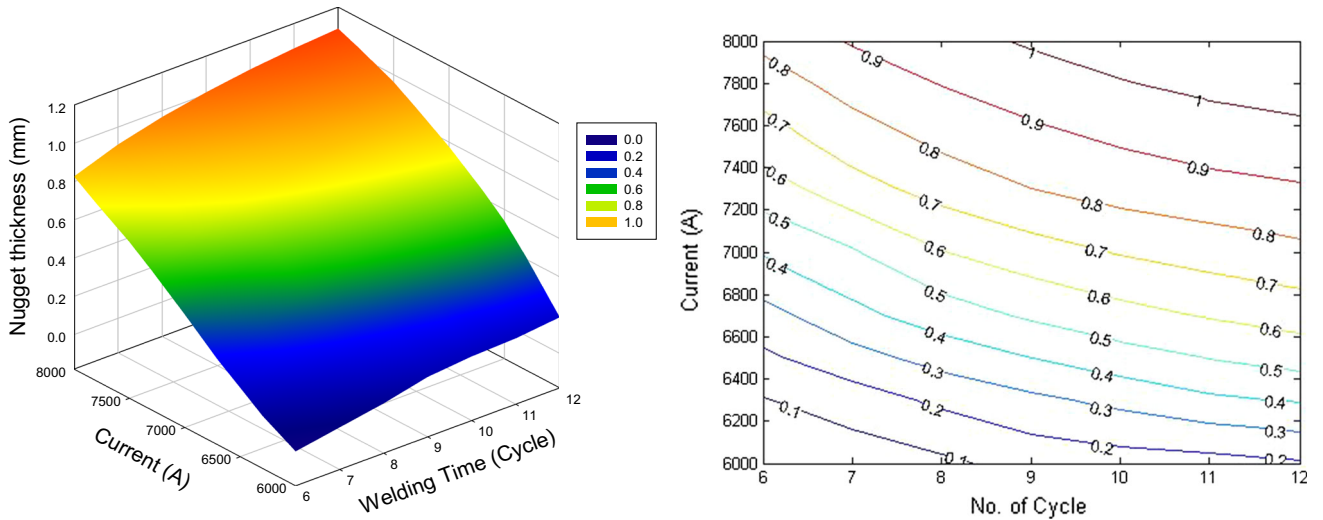


Fig. 15—Interaction between welding time, welding current, and nugget thickness with an electrode tip diameter of 4.7 mm.

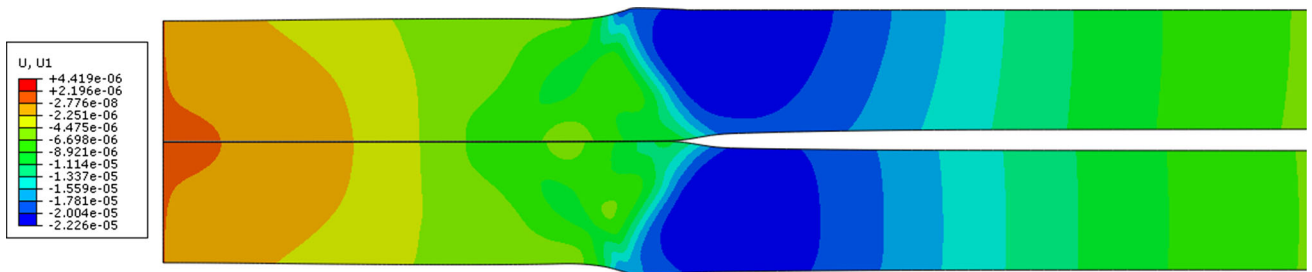


Fig. 16—The deformation of the weldment at the end of welding at the 10 cycles and 7 kA (amplified by 3 times).

proved that the parameters used in the welding process were chosen appropriately.

Figure 16 shows electrode indentation and sheet deformation after RSW process. The deformation will affect the properties of the welded joint since it cannot be completely eliminated after welding. For example, a fatigue crack or failure notch may initiate at the end of the gap between the two sheets (sheet separation), and electrode indentation is a place for stress concentration. As well as increasing the electrode indentation leads to the increase in contact surface of water-cooled copper electrode system to welding zone, and therefore the rate of cooling is increased with increasing the heat input. This subject is the main reason of microstructure refining and hardness increasing at the welding zone and HAZ which control the strength of spot welds.^[25]

Figure 17 illustrates that the depth of the electrode indentation values increased slowly at low current values, while they exhibited a relatively rapid increase at high current values. This increase was associated with the rise in the heat input observed in increasing welding currents. The depth of the electrode indentations had primary relevance to the fusion occurring in the weld nucleus. The result foreseen is that the depth of the electrode indentation will increase as the fusion amount in weld area increases.^[26]

Figure 18 shows the effect of electrode tip diameter and welding current on maximum temperature of the

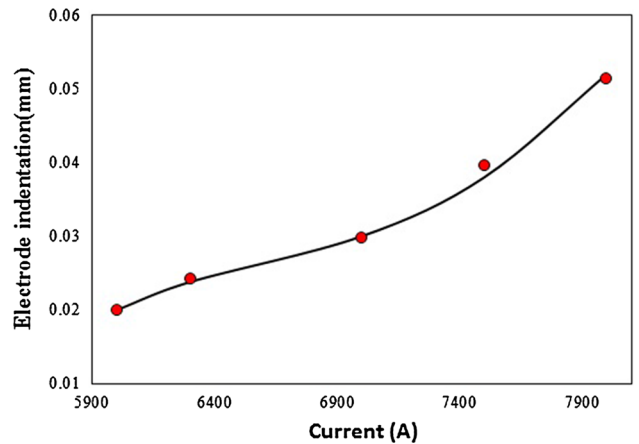


Fig. 17—The variation in the electrode indentation depths with the weld current at the welding time of 10 cycles.

nugget. It is clear from this figure that the maximum temperature of nugget increases with the decreasing electrode tip diameter and increasing welding current. Indeed, temperature of nugget sharply rises with increasing current density due to decreased contact area.

Paying attention to the diameter of the contact surface of electrode and workpieces or electrode tip diameter is important in RSW process that can affect the current density and thus the shape and size of the nugget

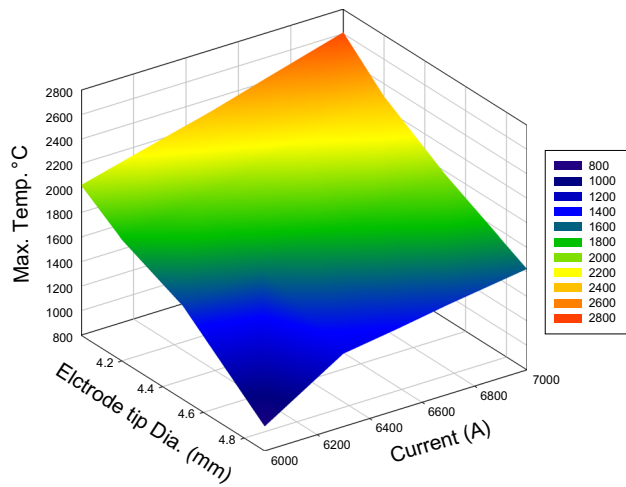


Fig. 18—Interaction between electrode tip diameter, welding current, and maximum temperature of nugget at the welding time of 10 cycles.

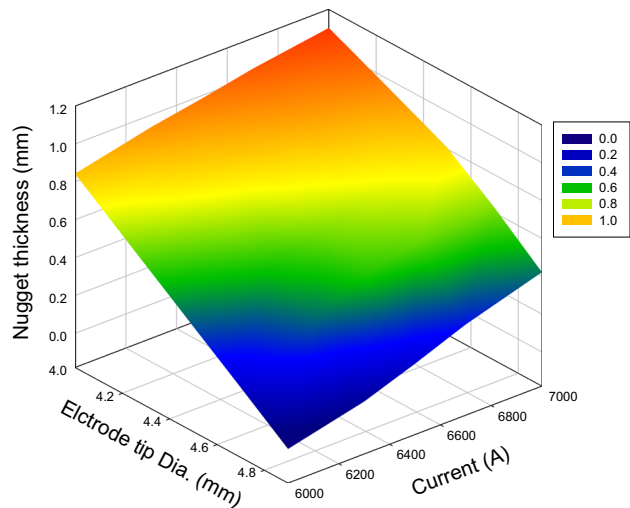


Fig. 20—Interaction between electrode tip diameter, welding current, and nugget thickness at the welding time of 10 cycles.

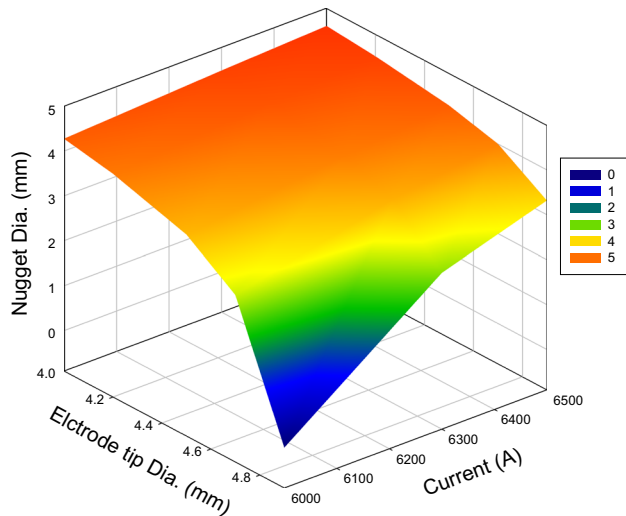


Fig. 19—Interaction between electrode tip diameter, welding current, and nugget diameter at the welding time of 10 cycles.

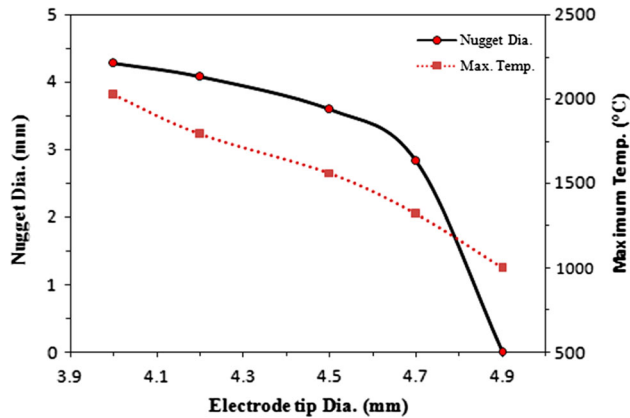


Fig. 21—The variation in the nugget diameter and maximum nugget temperature with the electrode tip diameter at the 6 kA welding current and the welding time of 10 cycles.

and electrode life. Figures 19 and 20 show the interaction effect of welding current and electrode tip diameter on nugget diameter and nugget thickness, respectively. As shown in Figure 19, with increasing the electrode tip diameter (at a constant welding current), nugget diameter becomes smaller, and in the higher current level this reduction is less. These subjects are discussed in two aspects. With reducing the diameter of electrode tip, the contact area between the two sheets or electrode and sheet diminishes, therewith the current density would be increased in these areas. On the other hand, under constant electrode force, a decrease in this parameter causes increasing applied pressure and reduced the contact resistivity of the interface sheets. But according to Joule equation the effect of current is greater than resistance. Figure 20 shows the interaction effect of welding current and electrode tip diameter on nugget thickness. Comparing Figures 19 and 20, it is clear that

when the electrode tip diameter decreases, the rate of increasing nugget thickness is much higher than that of the nugget diameter.

Figure 21 shows the effects of electrode tip diameter on maximum temperature of the nugget and nugget diameter under a welding current of 6 kA. It is obvious that when the electrode tip diameter has been increased further than 4.7 mm, the nugget cannot be formed. This figure also shows that the maximum temperature of nugget decreases with increasing electrode tip diameter, due to reduced current density and increased heat transfer by electrodes. Experimental and simulation results show that other remarkable phenomena that should be noted in choosing electrode diameter are expulsion, electrode erosion, and sheet deformation. Electrode diameter will create a mechanical barrier around the molten metal to keep the material within the nugget area. So in smaller electrode tip diameter (under constant current intensity), expulsion occurred earlier and maximum nugget diameter that can be achieved is smaller. Sheet deformation increases and electrode life

decreases because of increasing pressure and temperature with smaller electrode tip diameter. From the results, it is concluded that the best selection of electrode tip diameter is 4.7 mm for RSW of Inconel 625 with 0.7 mm thickness. Comparison between experimental and simulation results shows that the average error of FE model is less than 1.55 pct and the maximum error of FE model is 3.91 (at a welding current of 6 kA and welding time of 10 cycles).

VI. CONCLUSIONS

In this study, two-dimensional finite element simulation of RSW process was carried out using fully coupled electrical–thermal and uncoupled thermal–mechanical analyses on Inconel 625 sheets to predict weld nugget formation and electrode indentation through temperature distributions at different welding current intensities, cycles, and electrode tip diameter. The simulation results have been validated by the experimental results. In the span without expulsion occurrence, good agreement has been obtained between the predicted results and the measured data. The following essential conclusions can be drawn from this study:

1. Here, an uncoupled thermal–mechanical analysis was used instead of coupled thermal–mechanical analysis which has not been used in most of the previous works on simulation of RSW. This model is easier than coupled FE modeling and obtained similar trend of the effect of welding time and welding current on nugget size for Inconel 625, for both experiments and FE analysis results.
2. When welding time increases, temperature of faying surface of sheets rises rapidly until this area is melted and nugget is formed. After the formation of the nugget, the rate of temperature rise is reduced suddenly that is because increasing the welding time can enhance heat transfer to the surroundings, and therefore less heat is consumed in the formation of weld nugget.
3. As the welding current goes beyond a critical value for nugget formation, it causes a rapid growth of nugget. The nugget growth rate decreases as the welding current increases, but the nugget size increases until expulsion occurs. Expulsion causes a rapid growth of electrode indentation.
4. With increasing current density, the electrode indentation and increasing rate of this parameter increase because of poor mechanical properties due to higher temperature; but when electrode tip diameter has been increased, nugget diameter and electrode indentation decrease.

5. Finally, the results show that the developed FE model gives a precise estimate (with the average error less than 1.55 pct) for the nugget size and can be reliably used to numerically simulate the RSW of Inconel 625 alloy.

REFERENCES

1. H. Eisazadeh, M. Hamed, and A. Halvae: *Mater. Des.*, 2010, vol. 31, pp. 1149–57.
2. D. Li, Q. Guo, S. Guo, H. Peng, and Z. Wu: *Mater. Des.*, 2011, vol. 32, pp. 696–705.
3. M. Sundararaman, L. Kumar, P.G. Esvar, P. Mukhopadhyay, and S. Banerjee: *Metall. Mater. Trans. A*, 1992, vol. 30A, pp. 41–52.
4. S. Aslanlar: *Mater. Des.*, 2006, vol. 27, pp. 125–31.
5. H.A. Nied: *Weld. J. Re. Suppl.*, 1984, vol. 63, pp. 123–32.
6. P.S. Wei and C.Y. Ho: *ASME J. Heat Transfer*, 1990, vol. 112, pp. 316–90.
7. C.L. Tsai, O.A. Jammel, J.C. Papritan, and D.W. Dickinson: *Weld. J.*, 1992, vol. 71, pp. 47–54.
8. M. Vogler: *Weld. J.*, 1993, vol. 72, pp. 226–31.
9. S.M. Darwish and S.D. Al-Dkhial: *Int. J. Mach. Tools Manuf.*, 1999, vol. 39, pp. 1589–610.
10. X. Sun and P. Dong: *Weld. J.*, 2000, vol. 79, pp. 215–21.
11. Z. Hou, I. Kim, Y. Wang, C. Li, and C.J. Chen: *J. Mater. Process. Technol.*, 2007, vol. 180, pp. 160–65.
12. N. Ranjbar, S. Serajzadeh, and A.H. Kokabi: *J. Mater. Process. Technol.*, 2008, vol. 205, pp. 60–69.
13. Z. Lei, H. Kang, and Y. Liu: *Procedia Eng.*, 2011, vol. 16, pp. 622–31.
14. H. Moshayedi and I. Sattari-Far: *J. Mater. Process. Technol.*, 2012, vol. 212, pp. 347–54.
15. J. Shen, Y. Zhang, X. Lai, and P.C. Wang: *Mater. Des.*, 2011, vol. 32, pp. 550–60.
16. M. Eshraghi, M.A. Tschopp, M.A. Zaeem, and S.D. Felicelli: *Mater. Des.*, 2014, vol. 56, pp. 387–97.
17. R.S. Florea, K.N. Solanki, D.J. Bammann, J.C. Baird, J.B. Jordon, and M.P. Castanier: *Mater. Des.*, 2012, vol. 34, pp. 624–30.
18. B.H. Chang and Y. Zhou: *J. Mater. Process. Technol.*, 2003, vol. 139, pp. 635–41.
19. A.W. Society: Recommended Practices for Test Methods for Evaluating the Resistance Spot Welding Behavior of Automotive Sheet Steel Materials, ANSI/AWS/SAE/D89-97, Miami, ML (USA): AWS; 1997.
20. ASTM E 340-00, Reapproved 2006, Standard Test Method for Macroetching Metals and Alloys, ASTM International, USA.
21. H. Zhigang, W. Yuanxun, L. Chunzhi, and C.H. Chuanyao: *Acta Mech. Solida Sin.*, 2006, vol. 19, pp. 86–94.
22. D. Deng, H. Murakawa, and W. Liang: *Comp. Mater. Sci.*, 2008, vol. 42, pp. 234–44.
23. P.S. Wei and T.H. Wu: *Inter. J. Heat Mass. Trans.*, 2012, vol. 55, pp. 3316–24.
24. S.M. Hamidinejad, F. Kolahan, and A.H. Kokabi: *Mater. Des.*, 2012, vol. 34, pp. 759–67.
25. F. Khodabakhshi, M. Kazeminezhad, and A.H. Kokabi: *Mater. Charact.*, 2012, vol. 69, pp. 71–83.
26. F. Hayat: *Mater. Des.*, 2011, vol. 32, pp. 2476–84.